



This is the accepted manuscript made available via CHORUS, the article has been published as:

## Phase diagram of Nambu–Jona-Lasinio model with dimensional regularization

T. Inagaki, D. Kimura, H. Kohyama, and A. Kvinikhidze  
Phys. Rev. D **86**, 116013 — Published 28 December 2012

DOI: [10.1103/PhysRevD.86.116013](https://doi.org/10.1103/PhysRevD.86.116013)

# Phase diagram of Nambu–Jona-Lasinio model with dimensional regularization

T. Inagaki

*Information Media Center, Hiroshima University, Higashi-Hiroshima, Hiroshima 739-8521, Japan*

D. Kimura

*Faculty of Education, Hiroshima University, Higashi-Hiroshima, Hiroshima 739-8524, Japan*

H. Kohyama

*Department of Physics, Chung-Yuan Christian University, Chung-Li 32023, Taiwan*

A. Kvinikhidze

*A. Razmadze Mathematical Institute of Georgian Academy of Sciences,  
M. Alexidze Str. 1, 380093 Tbilisi, Georgia*

Regularization dependence of the NJL model leaves the room for its improvement. To help choosing a suitable regularization scheme we investigate the phase diagram on temperature-chemical potential plane in the Nambu–Jona-Lasinio model with the dimensional regularization. While the structure of the resulting diagram shows resemblance to the one in the frequently used cutoff regularization, some results of our study indicate striking difference between these regularizations. Diagrams in the dimensional regularization always indicate the first order phase transition at high chemical potential, while the first order transition does not occur in the cutoff method for some parameter sets.

PACS numbers: 11.10.Wx, 11.30.Qc, 12.39.-x

## I. INTRODUCTION

The phase diagram of the quark matter has been actively investigated for decades [1]. Quarks are confined inside hadrons and can not be observed as free particles at low energy. On the other hand at high energy, quarks become free particles due to the asymptotic freedom of the strong interaction. Therefore, it is expected that quarks undergo the phase transition between confined and deconfined states which is one of the most important issues in the theoretical and experimental particle physics.

The fundamental theory to describe quark matter is quantum chromodynamics (QCD), the theory of strong interaction. It is, however, not practical to extract reliable predictions at low energy due to the necessity of complicated nonperturbative calculations in this area. For this reason some effective approaches are used such as the Nambu–Jona-Lasinio (NJL) model [2] and its Polyakov-loop incorporated version, the PNJL model [3], the linear sigma model [4], the chiral perturbation theory [5], the lattice QCD simulations [6].

In this letter, we will consider the NJL model known as a low-energy effective theory of QCD (for reviews, see, [7–10]). At low temperature,  $T$ , and chemical potential,  $\mu$ , constituent quarks are heavy due to the chiral symmetry spontaneous breaking while they are expected to be light at high  $T$  and/or  $\mu$  where the chiral symmetry is getting restored. Thus the quark system is closely related to the phenomenon of the chiral phase transition. The NJL model actually predicts the chiral symmetry breaking at low energy and its restoration at high energy. Many investigations of the phase diagram are based on the NJL

and PNJL models (see, e.g., [11–20] and [21–25]).

Since the NJL model is not renormalizable, the model predictions inevitably depend on a regularization procedure applied. The most frequently used method is probably the three-momentum cutoff regularization which introduces the cutoff scale  $\Lambda$ . The model in the cutoff scheme may miss an important contribution when the quark density becomes comparable to the cutoff scale. There is an alternative method, the dimensional regularization (DR) [19, 26–28], to avoid the issue [29]. In the DR, divergences coming from fermion loop integrals are regularized by lowering the dimension of the integration through an analytic continuation in the dimension variable. The DR preserves gauge symmetry and chiral symmetry, as well as Lorentz invariance. Thus the DR method respects more symmetries than the cutoff method.

Using various regularization ways is interesting, because we believe that the regularization scheme is a dynamical part of the NJL model, it is related to the effective size and shape of the quark interaction as discussed in [31]. Thus the choice of regularization has direct effect on the reliability of the NJL model. It was found that the model with the DR nicely describes quark systems at low energy, such characteristics as the phase structure and meson properties [29–32]. Note that if we take some assumptions, the Schwinger-Dyson equation coincides with the gap equation in the two-dimensional NJL model at the leading order of  $1/N_c$  expansion [33].

We shall study in this article the phase diagram in the three flavor NJL model with the DR. It is interesting because the recent work by the present authors [31] indicates that the phase structure, especially the order of

the transition, may differ drastically from the one in the cutoff regularization.

The structure of this letter is following: In Sec. II, the three flavor NJL model and its parameters are presented. Section III is devoted to the explanation on the procedure of drawing the phase diagram. We then display the resulting phase diagram of the model in Sec. IV. We also evaluate the Columbia plot for two regularization methods in Sec. V. The concluding remarks are given in Sec. VI.

## II. THREE FLAVOR NJL MODEL

### A. The model

The Lagrangian of the three flavor model is

$$\mathcal{L}_{\text{NJL}} = \sum_{i,j} \bar{q}_i (i\cancel{\partial} - \hat{m})_{ij} q_j + \mathcal{L}_4 + \mathcal{L}_6, \quad (1)$$

$$\mathcal{L}_4 = G \sum_{a=0}^8 \left[ \left( \sum_{i,j} \bar{q}_i \lambda_a q_j \right)^2 + \left( \sum_{i,j} \bar{q}_i i\gamma_5 \lambda_a q_j \right)^2 \right], \quad (2)$$

$$\mathcal{L}_6 = K [\det \bar{q}_i (1 - \gamma_5) q_j + \text{H.c.}]. \quad (3)$$

where  $\hat{m}_{ij}$  represents the diagonal mass matrix  $\text{diag}(m_u, m_d, m_s)$  with flavor indices  $i, j$ .  $G$  and  $K$  are the four- and six-fermion couplings,  $\lambda_a$  are the Gell-Mann matrices in flavor space with  $\lambda_0 = \sqrt{2/3} \cdot \mathbf{1}$ . The determinant in  $\mathcal{L}_6$  runs over flavor space, so this leads to the six-point interaction known as Kobayashi-Maskawa 't Hooft (KMT) term [34, 35].

The vacuum of the model is determined by the minimum of the thermodynamic potential  $\Omega = -\ln Z/(\beta V)$  with the partition function  $Z$ , the inverse temperature  $\beta = 1/T$ , and the volume of the system  $V$ . Applying the mean-field approximation, we can calculate the potential  $\Omega$  in the imaginary time formalism,

$$\Omega_{\text{v}} = \Omega_0 + \Omega_T, \quad (4)$$

$$\Omega_{\text{F}} = 2G(\phi_u^2 + \phi_d^2 + \phi_s^2) - 4K\phi_u\phi_d\phi_s, \quad (5)$$

$$\Omega_{\text{F}} = \frac{2^{D/2} N_c}{2} \int \frac{d^{D-1}p}{(2\pi)^{D-1}} [E_u + E_d + E_s], \quad (6)$$

$$\Omega_{\text{F}} = \frac{2^{D/2} N_c T}{2} \int \frac{d^{D-1}p}{(2\pi)^{D-1}} \sum_{i,\pm} \ln [1 + e^{-\beta E_i^\pm}]. \quad (7)$$

Here  $\Omega_{\text{v}}$  corresponds to the vacuum contribution by the chiral condensates,  $\Omega_0$  and  $\Omega_T$  denote the temperature independent and dependent contributions,  $\phi_i (\equiv \langle \bar{i}i \rangle)$  is the chiral condensate for each quark which is the order parameter of the model,  $N_c (= 3)$  is the number of colors.  $D$  denotes dimensions in the fermion loop integral,  $E_i = (p^2 + m_i^{*2})^{1/2}$  is the energy of the quasi-particle with the constituent quark mass  $m_i^*$ ,  $E_i^\pm = E_i \pm \mu$  with a quark chemical potential  $\mu (= \mu_u = \mu_d = \mu_s)$ .

The fermion loop integral in Eq. (6) diverges, therefore we will perform the analytic continuation in  $D$  to

regularize it by decreasing the dimension  $D$  as discussed in [30, 31]. In the cutoff scheme, the divergent contribution is dropped by introducing the momentum cutoff  $\Lambda$ . To be more precise, the regularization in the DR and cutoff schemes are performed by the following replacements

$$\int \frac{d^{D-1}p}{(2\pi)^{D-1}} \frac{2(4\pi)^{-(D-1)/2}}{\Gamma[(D-1)/2]} M_0^{4-D} \int_0^\infty dp p^{D-2}, \quad (8)$$

$$\int \frac{d^{D-1}p}{(2\pi)^{D-1}} \frac{1}{2\pi^2} \int_0^\Lambda dp p^2, \quad (9)$$

where  $M_0$  is the renormalization scale which is needed to render physical quantities correct mass dimensions.

As mentioned in the introduction, the constituent quark mass

$$m_i^* = m_i - 4G\phi_i + 2K\phi_j\phi_k, \quad (i \neq j \neq k \neq i) \quad (10)$$

is closely related to the chiral symmetry breaking, namely to the value of  $\phi_i$ . The self-consistent gap equations (10) are obtained as the condition for the thermodynamic potential to be at the extremum,  $\partial\Omega/\partial\phi_i = 0$ . Equations (10) explicitly show that the difference between constituent and current quark masses is due to the underlying chiral symmetry breaking.

It is worth mentioning that the anomalous  $U_A(1)$  transformation can be used to ensure that all quark masses are positive. However, the  $U_A(1)$  transformation leads the positive chiral condensates which are not consistent with the study of QCD sum rules [36]. The sign of the mass should be studied when considering CP violating gauge couplings [37]. The detailed arguments on the  $U_A(1)$  transformation and the CP problem are discussed in the Appendix A. The sign of constituent quark masses do not change the phase diagram of the chiral transition in the NJL model.

Note that the constituent quark masses can be positive if one performs the renormalization by introducing counter terms which are necessary to eliminate the divergences coming from loop integrals [38]. However, the renormalized models in DR generate results similar to those in the cutoff method, which is not of our interest in this paper.

### B. Model parameters

The NJL model with the DR has 7 free parameters: current quark mass  $m_u, m_d, m_s$ , the four- and six-point couplings  $G, K$ , the dimension  $D$ , and the renormalization scale  $M_0$ .

We consider, for simplicity, the isospin symmetric case,  $m_d = m_u$ , and set several values for  $m_u (= 3, 4, 5, 5.5, 6 \text{ MeV})$ . We then fix the remaining parameters by choosing 5 physical quantities among listed below:

$$\begin{aligned} m_\pi &= 138 \text{ MeV}, & f_\pi &= 92 \text{ MeV}, \\ m_K &= 495 \text{ MeV}, & m_{\eta'} &= 958 \text{ MeV}, \\ m_\eta &= 548 \text{ MeV}, & \chi^{1/4} &= 170 \text{ MeV}. \end{aligned} \quad (11)$$

Following [31], we name the parameter sets as Case  $\chi$  and  $m_\eta$  depending on which quantities are selected. The Case  $\chi$  ( $m_\eta$ ) is fitted by  $\{m_\pi, f_\pi, m_K, m_{\eta'}, \chi(m_\eta)\}$ . The parameter setting was performed in [30], and we shall employ three parameter sets, Case  $m_\eta^{\text{LD}}$ ,  $m_\eta$  and  $\chi$ , which are shown in Tables I, II and III. Note that the Case  $m_\eta$

TABLE I. Case  $m_\eta^{\text{LD}}$ .

$m_u$	$m_s$	$G$	$K$	$M_0$	$D$
3.0	84.9	-0.0195	$9.02 \times 10^{-7}$	118	2.29

TABLE II. Case  $m_\eta$ .

$m_u$	$m_s$	$G$	$K$	$M_0$	$D$
3.0	79.0	-0.0130	$2.29 \times 10^{-7}$	107	2.37
4.0	106	-0.00748	$8.26 \times 10^{-8}$	92.0	2.52
5.0	134	-0.00357	$1.99 \times 10^{-8}$	73.2	2.69
5.5	147	-0.00231	$8.40 \times 10^{-9}$	62.4	2.77
6.0	162	-0.00142	$3.23 \times 10^{-9}$	50.9	2.87

TABLE III. Case  $\chi$ .

$m_u$	$m_s$	$G$	$K$	$M_0$	$D$
3.0	77.1	-0.0168	$2.23 \times 10^{-7}$	120	2.28
4.0	106	-0.0143	$2.11 \times 10^{-7}$	116	2.36
5.0	134	-0.0119	$1.80 \times 10^{-7}$	112	2.43
5.5	150	-0.0109	$1.62 \times 10^{-7}$	110	2.47
6.0	166	-0.00992	$1.48 \times 10^{-7}$	109	2.50

has two parameter sets for  $m_u = 3\text{MeV}$ ; to distinguish between them we use the superscript LD (lower dimension).

For the sake of comparison we also align the parameters of the cutoff case in Table IV. In the cutoff case, we fix 4 parameters,  $m_s, G, K$  and  $\Lambda$  with  $\{m_\pi, f_\pi, m_K, m_{\eta'}\}$ . Unfortunately, there is no solution to simultaneously reproduce the above listed quantities for  $m_u \gtrsim 5.87\text{MeV}$ .

TABLE IV. Case Cutoff.

$m_u$	$m_s$	$G\Lambda^2$	$K\Lambda^5$	$\Lambda$
3.0	89.5	1.55	8.34	960
4.0	110	1.60	8.38	797
5.0	128	1.71	8.77	682
5.5	136	1.81	9.17	630
5.87	139	2.09	10.1	580

### III. CRITICAL BEHAVIOR

In this section we explain how to draw the phase diagram of the model through the analysis of the thermodynamical potential and the gap equations.

A critical temperature  $T_c$  or chemical potential  $\mu_c$  are

given by the maxima of

$$\frac{\partial\phi_u}{\partial t}, \quad (t = T \text{ or } \mu). \quad (12)$$

To be precise, in the case of  $t = T$ , the critical temperature,  $T_c$ , is given by a value of  $T$  at which the two variable function,  $\partial\phi_u(\mu, T)/\partial T$ , reaches the maximum. Thus the critical temperature,  $T_c = T_c(\mu)$ , is a function of  $\mu$ . Analogously is defined the critical chemical potential,  $\mu_c(T)$ .

We apply  $t = T(\mu)$  for low  $\mu$  ( $T$ ) in crossover region. The above quantity,  $\partial\phi_u/\partial T$ , becomes infinite at  $T_c(\mu_c)$  when the transition is of the first order. In this case we determine the transition boundary by the point where the discontinuous change of the chiral condensate  $\phi_u$  occurs by directly searching the minimum of the thermodynamic potential. It is obvious that this procedure is consistent with the criterion of Eq. (12), because a divergent point coincides the maximum point.

#### A. Thermodynamic potential

To see the tendency of the phase transition, we show the behavior of  $\Omega(= \Omega(\phi_u, \phi_s) - \Omega(0, 0))$  for the Case  $m_\eta$  and Cutoff with  $m_u = 4\text{MeV}$  near the transition boundary in Fig. 1. The curves are plotted along the line  $\phi_s = 0.36\phi_u + 0.83\phi_u^0$  for  $T = 10, 75$  and  $85\text{MeV}$  with  $\mu = 480\text{MeV}$  in the upper panel, and along the line  $\phi_s = 0.103\phi_u + 1.43\phi_u^0$  for  $T = 10, 20, 30\text{MeV}$  with  $\mu = 290\text{MeV}$  in the lower panel. These lines are chosen so as to show the global minima for lower  $T = 75(10)\text{MeV}$  and higher  $T = 85(30)\text{MeV}$ , which are indicated by the circles, near the transition temperature  $T_c \simeq 80(20)\text{MeV}$ .  $\phi_u^0$  denotes the chiral condensate  $\phi_u$  at  $T, \mu = 0$  for each case.

There exists a bump between two stable minima in the DR case, which means that the transition is of the first order between  $T = 75$  and  $85\text{MeV}$  for  $m_u = 4\text{MeV}$  in the Case  $m_\eta$ . The shape of the potential with a bump does not change drastically if one chooses different parameter sets. On the other hand, the cutoff case (lower panel) produces rather monotonous curves with no bump when we choose the parameter sets with small value of  $m_u$ , which leads to a smooth crossover. This different tendency may stem from the fact that the ratio of the thermal contribution ( $\mu$  dependence)  $\Omega_T/(\Omega_v + \Omega_0)$  in the DR case is larger than that in the cutoff case at low  $T$ .

#### B. $\partial\phi_u/\partial T$

In the crossover region, it is technically easier to analyze Eq. (12) through solving the gap equations because  $\phi_u$  changes continuously with respect to  $T(\mu)$ . We show the numerical results in Fig. 2. One sees that the maximum point moves toward lower  $T$  with increasing  $\mu$ ,

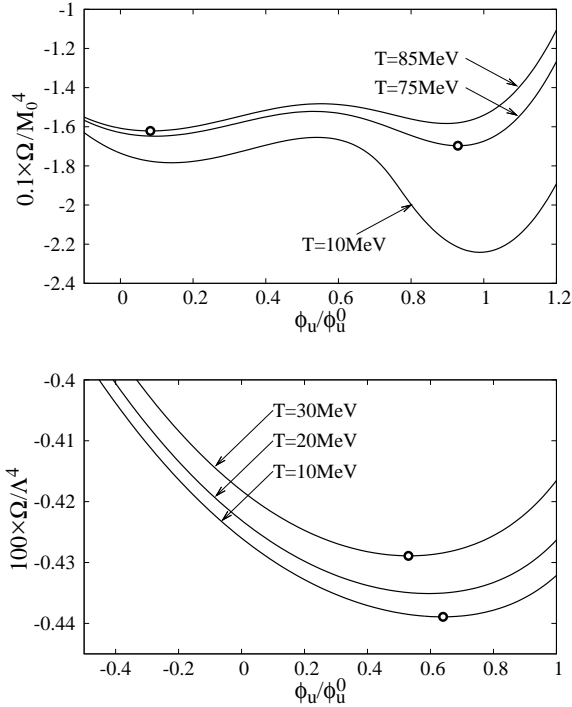


FIG. 1. Upper panel:  $0.1 \cdot \Omega / M_0^4$  along the line  $\phi_s = 0.36\phi_u + 0.83\phi_u^0$  in the Case  $m_\eta$  with  $m_u = 4\text{MeV}$  for  $T = 10, 75, 85\text{MeV}$  and  $\mu = 480\text{MeV}$ . Lower panel:  $100 \cdot \Omega / \Lambda^4$  along the line  $\phi_s = 0.103\phi_u + 1.43\phi_u^0$  in the Case Cutoff with  $m_u = 4\text{MeV}$  for  $T = 10, 20, 30\text{MeV}$  and  $\mu = 290\text{MeV}$ . Here  $\Omega = \Omega(\phi_u, \phi_s) - \Omega(0, 0)$  and  $\phi_u^0$  denotes the chiral condensate at  $T, \mu = 0$  for each case. The circles indicate the global minima.

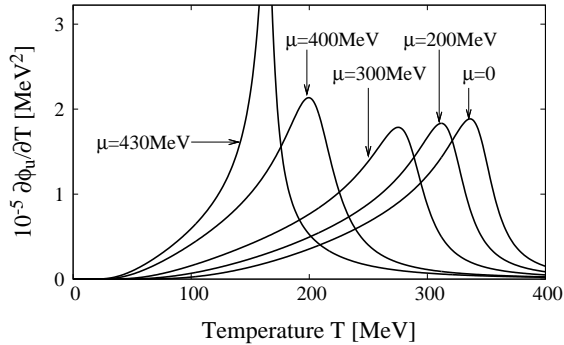


FIG. 2.  $\partial\phi_u/\partial T$  in the Case  $m_\eta$  with  $m_u = 4\text{MeV}$ .

and the peak becomes large at high  $\mu$ . The peak actually diverges when  $T$  and  $\mu$  coincide with the critical point  $(T_{CP}, \mu_{CP})$ . Below  $T_{CP}$ , the transition becomes of the first order, and the analysis by Eq. (12) is no longer practically useful for the determination of the transition boundary as mentioned above.

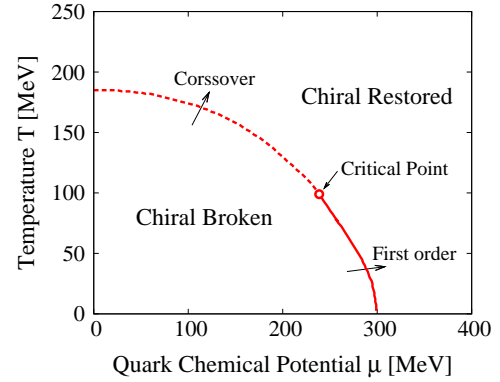


FIG. 3. Phase diagram in the Case  $m_\eta^{\text{LD}}$  with  $m_u = 3\text{MeV}$ . The solid (dashed) line represents the first order (crossover) transition. The circle indicates the critical point.

#### IV. PHASE DIAGRAM

We are now ready to discuss the phase structure of the NJL model with the DR.

##### A. Transition on $\phi_u$

Figure 3 displays the typical structure of the phase diagram in the model with the DR in the Case  $m_\eta^{\text{LD}}$ . This is a reasonable picture of a system in the chiral symmetry broken phase at low  $T$  and  $\mu$ , and in the chiral symmetry restored phase at high  $T$  and/or  $\mu$ . The solid (dashed) line represents the first order (crossover) transition, and the circle indicates the critical point. Note that the transition temperature,  $T_c = 184\text{MeV}$  for  $\mu = 0$ , is comparable with the lattice QCD prediction,  $150 - 200\text{MeV}$ . The critical point is located at  $(T_{CP}, \mu_{CP}) = (99\text{MeV}, 239\text{MeV})$ , and it is interesting to see that  $T_{CP}$  is close to one obtained in the PNJL model with the cutoff regularization,  $T_{CP} = 102\text{MeV}$ , for frequently used parameter set of [9], whereas  $T_{CP} = 48\text{MeV}$  in the NJL model [24]. Note that the obtained critical point is close to one obtained in a NJL type model with the smooth form factor [20],  $(T_{CP}, \mu_{CP}) = (101\text{MeV}, 211\text{MeV})$ , and in the linear sigma model [39],  $(T_{CP}, \mu_{CP}) = (99\text{MeV}, 207\text{MeV})$ . Below we make more detailed comparison between the DR and the cutoff schemes.

Figure 4 shows the phase diagrams in the Cases  $m_\eta$  and  $\chi$  for various  $m_u$ . We note that in the Case  $m_\eta$ , the region of chiral symmetry broken phase becomes smaller with choosing the smaller value of  $m_u$ . On the other hand the Case  $\chi$  produces similar curves for different  $m_u$ . The different behavior can be explained by the fact that the constituent quark mass  $m_u^*$  gets smaller with decreasing  $m_u$  in the Case  $m_\eta$ , while it almost does not change in the Case  $\chi$  as discussed in [30]. In the cutoff case (Fig. 5) the region of the chiral symmetry broken state shrinks

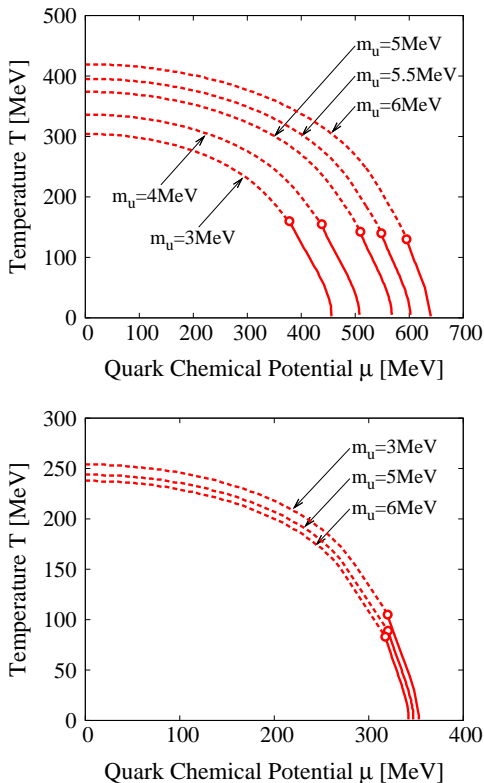


FIG. 4. Phase diagrams in the Case  $m_\eta$  and  $\chi$  are shown in the upper and lower panels. The solid (dashed) lines represent the first order (crossover) transition. The circles indicate the critical points.

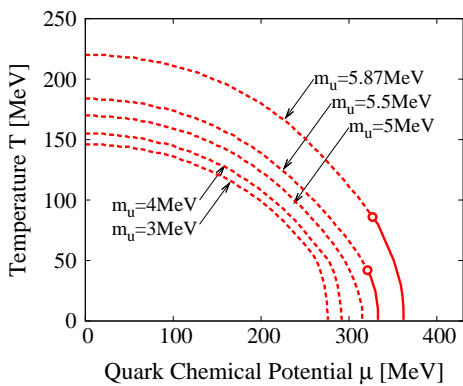


FIG. 5. Corresponding diagrams in the Case Cutoff.

when  $m_u$  is lowered as observed in the Case  $m_\eta$ . It is very interesting to note that the critical point disappears below  $m_u = 5\text{MeV}$ , where the transition is crossover for all  $T$  and  $\mu$ .

A striking difference between the two regularizations is in that the critical point moves towards higher temperature with decreasing  $m_u$  in the DR, while it moves to the opposite direction in the cutoff case. The difference may be understood by observing the value of the six-

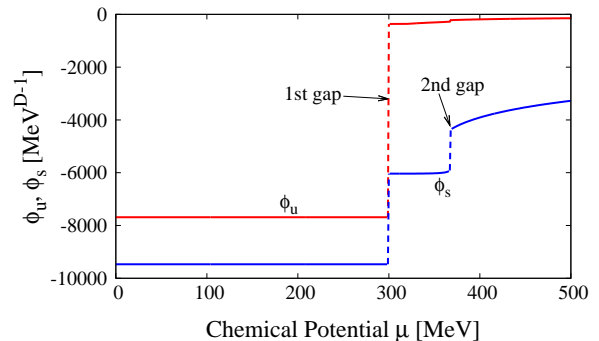


FIG. 6. Chiral condensates  $\phi_u$  and  $\phi_s$  for  $T = 10\text{MeV}$  in the Case  $m_\eta^{\text{LD}}$  with  $m_u = 3\text{MeV}$ .

point coupling  $K$  which becomes larger (smaller) with decreasing  $m_u$  in the DR (cutoff) procedure, since the KMT term shown in Eq.(3) tends to drive the first order phase transition [24].

### B. Partial transition on $\phi_s$

As discussed in [31] chiral condensates undergo two discontinuous changes at low  $T$  in the DR scheme. Figure 6 displays the typical behavior of  $\phi_u$  and  $\phi_s$  as functions of  $\mu$  at low  $T$  ( $= 10\text{MeV}$ ), plotted in the Case  $m_\eta^{\text{LD}}$  with  $m_u = 3\text{MeV}$ . One clearly observes two gaps: one is located around  $\mu_c^{(u)} \simeq 300\text{MeV}$  and the other is around  $\mu_c^{(s)} \simeq 365\text{MeV}$ . Here we call these discontinuities as first and second gaps for lower and higher chemical potential, respectively. The first gap comes from the effect of the approximate  $\text{SU}_L(2) \otimes \text{SU}_R(2)$  restoration and the second one comes from that of the partial  $\text{SU}_L(3) \otimes \text{SU}_R(3)$  restoration. Two gaps are also observed in NJL model with the cutoff regularization under the charge neutrality condition [40]. Thus it may be interesting to study the phase structure concerning the second transition as well.

To draw the phase diagram on the second transition, we set the criterion of the transition by using the following quantity

$$\frac{\partial \phi_s}{\partial t}, \quad (t = T \text{ or } \mu). \quad (13)$$

Then below  $\mu_{\text{CP}}$ , namely in the crossover region, the above quantity has only one maximum, which determines the crossover transition on  $\phi_s$ . While above  $\mu_{\text{CP}}$  the quantity  $\partial \phi_s / \partial \mu$  shows non-trivial behavior; it becomes infinite at  $\mu_c^{(u)}$ , and has second maximum at  $\mu_c^{(s)}$ . So  $\partial \phi_s / \partial \mu$  has typical two maxima at  $\mu_c^{(u)}$  and  $\mu_c^{(s)}$  below  $T_{\text{CP}}$  as seen in Fig. 6. Here we call the transition point corresponding to the second maximum,  $\mu_c^{(s)}$ , “the second phase boundary”. To distinguish between the two phase transitions, we call the transition line on  $\phi_u$  discussed in the previous subsection “the first phase boundary”.

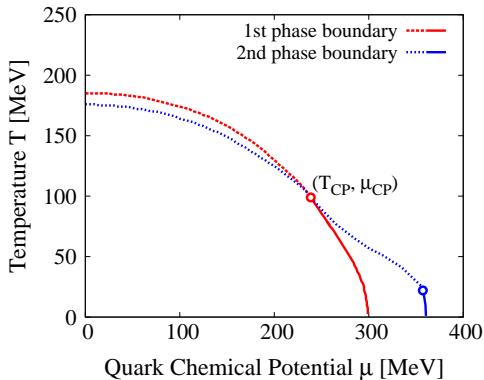


FIG. 7. The 1st and 2nd phase boundaries in the Case  $m_\eta^{\text{LD}}$  with  $m_u = 3\text{MeV}$ . The red dashed and blue dotted lines represent the crossover transition on  $\phi_u$  and  $\phi_s$ . The red and blue solid lines indicate the transition on the first and second gap, respectively. The circles exhibit the critical points.

In the phase diagram on the 1st and 2nd phase boundaries (Fig. 7) the dashed and dotted lines represent the crossover transition on  $\phi_u$  and  $\phi_s$ , respectively. The solid line for lower (higher) chemical potential indicates the discontinuous change on the first (second) gap. We see that the crossover line on  $\phi_s$  is observed at a bit lower temperature than that on  $\phi_u$  for  $\mu < \mu_{\text{CP}}$ . It should be noticed that the critical curves on  $\phi_u$  and  $\phi_s$  intersect at the critical end point  $(T_{\text{CP}}, \mu_{\text{CP}})$  on  $\phi_u$ . Because the value of  $\phi_s$  is affected by  $\phi_u$ , as is clearly seen from Fig. 6,  $\phi_s$  shows discontinuous change at the point where  $\phi_u$  has a gap. Then  $\partial\phi_s/\partial t$  blows up and approaches to infinity near the critical point where  $\partial\phi_u/\partial t$  is divergent. Below  $T_{\text{CP}}$ ,  $\partial\phi_s/\partial\mu$  has two maxima appearing at the first gap and higher chemical potential. The first maximum coincides with the red solid line and the second one is plotted by the blue line in Fig. 7. The transition on the second boundary also has the critical point whose location is exhibited by the blue circle at higher chemical potential.

We also studied the other Cases,  $m_\eta$  and  $\chi$ , with various  $m_u$ , and found that the qualitative behavior does not show remarkable difference; the critical point on  $\phi_s$  moves toward higher temperature with decreasing  $m_u$  as seen in the  $\phi_u$  case. Therefore, we only displayed the Case  $m_\eta^{\text{LD}}$  here.

## V. CRITICAL BOUNDARY

Having obtained the phase diagram for the NJL model in the DR scheme, it may be interesting to discuss the chiral critical boundary, so called Columbia plot [41]. The critical boundary is drawn by searching the order of the phase transition for various  $m_u$  and  $m_s$  while the remaining parameters discussed in Sec. II B are fixed. Thus the current quark masses,  $m_u$  and  $m_s$ , are treated as free

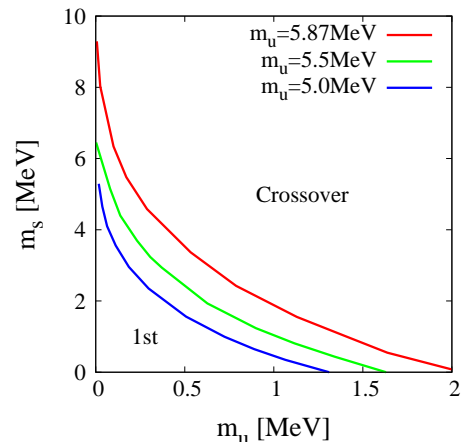
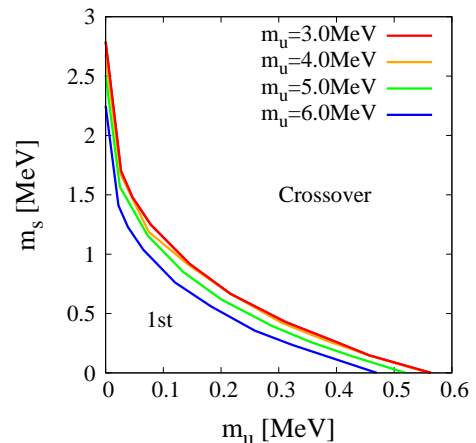


FIG. 8. The critical boundary for the Case  $m_\eta$  and Cutoff.

parameters when one studies the critical boundary.

The figure 8 displays the critical boundary for the Case  $m_\eta$  (upper panel) and Cutoff (lower panel) for various  $m_u$ . We first note that the values of the critical mass in the DR are considerably smaller than in the cutoff case with  $m_u = 5.0$  and  $5.5\text{MeV}$ . We also note that the region of the first order phase transition in the Case  $m_\eta$  does not depend drastically on the choice of the parameter sets. However the first order phase transition region shrinks with decreasing  $m_u$  and disappears at  $m_u = 4\text{MeV}$  in the Case Cutoff. This is a sharp contrast seen between the cases with DR and Cutoff regularization.

We have also evaluated the critical boundary for the Case  $m_\eta^{\text{LD}}$  and  $\chi$ , and found that the obtained curves indicate similar pictures with the Case  $m_\eta$ . Here we have only shown the results for the Case  $m_\eta$ .

## VI. CONCLUDING REMARKS

We studied the phase diagram of the NJL model with the DR and cutoff regularization. We found that the phase diagram on the  $T - \mu$  plane in the model with the DR for various parameter sets shows qualitatively

similar pictures. The typical transition temperatures are around 170, 350, 250 and 170MeV in the Case  $m_\eta^{\text{LD}}$ ,  $m_\eta$ ,  $\chi$  and Cutoff, respectively. The critical points are located around  $T_{\text{CP}} = 100 - 150\text{MeV}$  in the DR, and  $T_{\text{CP}} = 50 - 100\text{MeV}$  in the cutoff method. Interestingly enough, the temperature of the critical point  $T_{\text{CP}}$  increases with decreasing  $m_u$  in the DR case, while it rapidly becomes small in the cutoff case as confirmed in Fig 5. This is a sharp qualitative difference between the two cases.

In the Sec. V we drew the Columbia plot for the case of DR and cutoff regularization to study the order of phase transition in more detail. We saw that in the Columbia plot ( $\mu = 0$ ), the cutoff way leads to a larger region of the first order phase transition than that of the DR. However the first order transition region disappears when one chooses the parameter sets with smaller  $m_u$  in the cutoff case. On the other hand, the first order transition region remains in the DR, which is again the distinguishing difference between the two regularizations.

We have also studied the phase structure on the change of  $\phi_s$  in Sec. IV B, where we found that the approximate  $\text{SU}_L(2) \otimes \text{SU}_R(2)$  symmetry and the partial  $\text{SU}_L(3) \otimes \text{SU}_R(3)$  symmetry restore at a similar temperature for low chemical potential,  $\mu < \mu_{\text{CP}}$ . It may be difficult to distinguish between the two lines experimentally, because the transitions are smooth crossover at low chemical potential.

From the obtained phase diagrams and the Columbia plot, we conclude that the first order phase transition persists for low  $m_u$  in the model with the DR method. The finding is consistent with the current symmetry analysis based consensus [42] stating that the chiral phase transition is of the first order in the chiral limit,  $m_{u,d,s} \rightarrow 0$ . This tendency may be understood by the following reasoning. The loop contribution from the lower integration momenta is enhanced by lowering dimension. It introduces non-locality in the model with the DR. The infrared behavior of the loop integral is important for thermal corrections. It can rise the critical end point temperature,  $T_{\text{CP}}$ .

Finally, because the parameter difference crucially affects the location of the critical point as confirmed in this article, we think it is interesting to study the related

issues, such as the case with the chiral limit and the analysis in the next to the leading order approximation of the  $1/N_c$  expansion.

## ACKNOWLEDGMENTS

H. K. is supported by the Grant No. NSC-99-2811-M-033-017 from National Science Council (NSC) of Taiwan. A. K. was supported by Georgian Shota Rustaveli National Science Foundation (grant Nr. 11/31).

### Appendix A: $U_A(1)$ and strong CP violation

We start from a primordial  $\theta$ -term,

$$\mathcal{L}_\theta = \frac{g_s^2}{16\pi^2} \theta \epsilon^{\mu\nu\rho\sigma} F_{\mu\nu}^a F_{\rho\sigma}^a, \quad (\text{A1})$$

where  $F_{\mu\nu}^a$  is the field strength for gluons, and  $g_s$  is the strong coupling constant. The anomalous  $U_A(1)$  transformation induces the following additional contribution,

$$\begin{aligned} \mathcal{L}'_\theta &= \frac{g_s^2}{16\pi^2} (\theta + \arg \det \hat{m}^*) \epsilon^{\mu\nu\rho\sigma} F_{\mu\nu}^a F_{\rho\sigma}^a \\ &= \frac{g_s^2}{16\pi^2} (\theta + \pi) \epsilon^{\mu\nu\rho\sigma} F_{\mu\nu}^a F_{\rho\sigma}^a, \end{aligned} \quad (\text{A2})$$

with  $\hat{m}^* = \text{diag}(m_u^*, m_d^*, m_s^*)$ . In evaluating the second line, we assumed that all the constituent quark masses are negative. The term breaks CP symmetry and generates the neutron electric dipole moment. The coefficient is experimentally constrained as [43],

$$\theta + \pi \lesssim 10^{-9}. \quad (\text{A3})$$

This is a fine tuning problem which is known as the strong CP problem [44].

Then the CP symmetry is almost restored after the chiral condensation. The primordial  $\theta$  may be tested in the phenomena at high  $T$  and  $\mu$  where the chiral symmetry is partially restored. One of these possibilities may be found in the process for the baryogenesis, while it is beyond the scope of the present study based on the NJL model.

- 
- [1] For recent reviews, M. A. Stephanov, Prog. Theor. Phys. Suppl. **153**, 139 (2004), Int. J. Mod. Phys. A **20**, 4387 (2005), PoS LAT **2006**, 024 (2006), O. Philipsen, Prog. Theor. Phys. Suppl. **174**, 206 (2008), arXiv:1111.5370 [hep-ph], W. Weise, Prog. Theor. Phys. Suppl. **186**, 390 (2010), arXiv:1201.0950 [nucl-th], K. Fukushima and T. Hatsuda, Rept. Prog. Phys. **74**, 014001 (2011), G. Endrodi, Z. Fodor, S. D. Katz and K. K. Szabo, JHEP **1104**, 001 (2011).
- [2] Y. Nambu and G. Jona-Lasinio, Phys. Rev. **122**, 345 (1961); **124**, 246 (1961).
- [3] K. Fukushima, Phys. Lett. B **591**, 277 (2004).
- [4] M. Gell-Mann and M. Levy, Nuovo Cimento **16**, 705 (1960).
- [5] J. Gasser and H. Leutwyler, Nucl. Phys. B **250**, 465 (1985).
- [6] K. G. Wilson, Phys. Rev. D **10**, 2445 (1974).
- [7] U. Vogl and W. Weise, Prog. Part. Nucl. Phys. **27**, 195 (1991).
- [8] S. P. Klevansky, Rev. Mod. Phys. **64**, 649 (1992).
- [9] T. Hatsuda and T. Kunihiro, Phys. Rept. **247**, 221 (1994).
- [10] M. Buballa, Phys. Rept. **407**, 205 (2005).
- [11] U. Wolff, Phys. Lett. B **157**, 303 (1985).

- [12] T. Hatsuda and T. Kunihiro, Phys. Rev. Lett. **55**, 158 (1985).
- [13] F. Karsch, J. B. Kogut and H. W. Wyld, Nucl. Phys. B **280**, 289 (1987).
- [14] K. G. Klimenko, Z. Phys. C **37**, 457 (1988).
- [15] M. Asakawa and K. Yazaki, Nucl. Phys. A **504**, 668 (1989).
- [16] B. Rosenstein, B. Warr and S. H. Park, Phys. Rept. **205**, 59 (1991).
- [17] S. Hands, A. Kocic and J. B. Kogut, Nucl. Phys. B **390**, 355 (1993).
- [18] P. Zhuang, J. Hufner and S. P. Klevansky, Nucl. Phys. A **576**, 525 (1994).
- [19] T. Inagaki, T. Kouno, and T. Muta, Int. J. Mod. Phys. A **10**, 2241 (1995).
- [20] J. Berges and K. Rajagopal, Nucl. Phys. B **538**, 215 (1999).
- [21] K. Fukushima, Phys. Rev. D **68**, 045004 (2003).
- [22] C. Ratti, M. A. Thaler and W. Weise, Phys. Rev. D **73**, 014019 (2006).
- [23] S. Roessner, C. Ratti and W. Weise, Phys. Rev. D **75**, 034007 (2007).
- [24] K. Fukushima, Phys. Rev. D **77**, 114028 (2008) [Erratum-ibid. D **78**, 039902 (2008)]
- [25] T. Hell, S. Roessner, M. Cristoforetti and W. Weise, Phys. Rev. D **79**, 014022 (2009), Phys. Rev. D **81**, 074034 (2010).
- [26] S. Krewald and K. Nakayama, Ann. Phys. **216**, 201 (1992); T. Inagaki, T. Kouno, and T. Muta, Int. J. Mod. Phys. A **10**, 2241 (1995).
- [27] S. I. Kruglov, Hadronic J. **26**, 425 (2003).
- [28] R.G. Jafarov and V.E. Rochev, Russ. Phys. J. **49**, (2006) 712.
- [29] T. Fujihara, D. Kimura, T. Inagaki, and A. Kvinikhidze Phys. Rev. D **79**, 096008 (2009).
- [30] T. Inagaki, D. Kimura, H. Kohyama, and A. Kvinikhidze, Phys. Rev. D **83**, 034005 (2011).
- [31] T. Inagaki, D. Kimura, H. Kohyama and A. Kvinikhidze, Phys. Rev. D **85**, 076002 (2012).
- [32] T. Inagaki, D. Kimura, and A. Kvinikhidze, Phys. Rev. D **77**, 116004 (2008).
- [33] T. Fujihara, T. Inagaki, D. Kimura and A. Kvinikhidze, Prog. Theor. Phys. Suppl. **174**, 72 (2008).
- [34] M. Kobayashi and T. Maskawa, Prog. Theor. Phys. **44**, 1422 (1970), M. Kobayashi, H. Kondo, and T. Maskawa, Prog. Theor. Phys. **45**, 1955 (1971),
- [35] G. 't Hooft, Phys. Rev. D **14**, 3432 (1976) [Erratum-ibid. D **18**, 2199 (1978)]; Phys. Rept. **142**, 357 (1986).
- [36] M. A. Shifman, Prog. Theor. Phys. Suppl. **131**, 1 (1998).
- [37] R. F. Dashen, Phys. Rev. D **3**, 1879 (1971).
- [38] T. Eguchi, Phys. Rev. D **17**, 611 (1978).
- [39] O. Scavenius, A. Mocsy, I. N. Mishustin and D. H. Rischke, Phys. Rev. C **64**, 045202 (2001).
- [40] S. B. Ruester, V. Werth, M. Buballa, I. A. Shovkovy and D. H. Rischke, Phys. Rev. D **72**, 034004 (2005).
- [41] F. R. Brown *et al.*, Phys. Rev. Lett. **65**, 2491 (1990).
- [42] R. D. Pisarski and F. Wilczek, Phys. Rev. D **29**, 338 (1984).
- [43] J. Beringer *et al.* [Particle Data Group Collaboration], Phys. Rev. D **86**, 010001 (2012).
- [44] H. -Y. Cheng, Phys. Rept. **158**, 1 (1988).